

Core structure and Peierls stress of the 90° dislocation and the 60° dislocation in aluminum investigated by the fully discrete Peierls model

Hao Xiang(向浩), Rui Wang(王锐), Feng-Lin Deng(邓凤麟), and Shao-Feng Wang(王少峰)
Citation: Chin. Phys. B, 2022, 31 (**8**): 086104. DOI: 10.1088/1674-1056/ac587f
Journal homepage: http://cpb.iphy.ac.cn; http://iopscience.iop.org/cpb

What follows is a list of articles you may be interested in

Introducing voids around the interlayer of AlN by high temperature annealing

Jianwei Ben(贲建伟), Jiangliu Luo(罗江流), Zhichen Lin(林之晨), Xiaojuan Sun(孙晓娟), Xinke Liu(刘新科), and Xiaohua Li(黎晓华)
Chin. Phys. B, 2022, 31 (**7**): 076104. DOI: 10.1088/1674-1056/ac3d7f

Evolution of defects and deformation mechanisms in different tensile directions of solidified lamellar Ti-Al alloy

Yutao Liu(刘玉涛), Tinghong Gao(高廷红), Yue Gao(高越), Lianxin Li(李连欣), Min Tan(谭敏), Quan Xie(谢泉), Qian Chen(陈茜), Zean Tian(田泽安), Yongchao Liang(梁永超), and Bei Wang(王蓓)
Chin. Phys. B, 2022, 31 (**4**): 046105. DOI: 10.1088/1674-1056/ac1f0b

Mechanism of microweld formation and breakage during Cu-Cu wire bonding investigated by molecular dynamics simulation

Beikang Gu(顾倍康), Shengnan Shen(申胜男), and Hui Li(李辉)
Chin. Phys. B, 2022, 31 (**1**): 016101. DOI: 10.1088/1674-1056/ac0e24

Microstructure evolution of T91 steel after heavy ion irradiation at 550 ℃

Ligang Song(宋力刚), Bo Huang(黄波), Jianghua Li(李江华), Xianfeng Ma(马显锋), Yang Li(李阳), Zehua Fang(方泽华), Min Liu(刘敏), Jishen Jiang(蒋季伸), and Yanying Hu(胡琰莹)
Chin. Phys. B, 2021, 30 (**8**): 086103. DOI: 10.1088/1674-1056/ac0a64

Effect of tellurium (Te^{4+}) irradiation on microstructure and associated irradiation-induced hardening

Hefei Huang(黄鹤飞), Jizhao Liu(刘继召), Guanhong Lei(雷冠虹), Ondrej Muránsky, Tao Wei, and Mihail Ionescu
Chin. Phys. B, 2021, 30 (**5**): 056108. DOI: 10.1088/1674-1056/abf039

Core structure and Peierls stress of the 90° dislocation and the 60° dislocation in aluminum investigated by the fully discrete Peierls model

Hao Xiang(向浩)[1], Rui Wang(王锐)[1], Feng-Lin Deng(邓凤麟)[2,3], and Shao-Feng Wang(王少峰)[1,†]

[1] *Department of Physics and Institute for Structure and Function, Chongqing University, Chongqing* 401331, *China*
[2] *CAS Key Laboratory of Magnetic Materials and Devices, Ningbo Institute of Materials Technology and Engineering, Chinese Academy of Sciences, Ningbo* 315201, *China*
[3] *Zhejiang Province Key Laboratory of Magnetic Materials and Application Technology, Ningbo Institute of Materials Technology and Engineering, Chinese Academy of Sciences, Ningbo* 315201, *China*

(Received 6 January 2022; revised manuscript received 14 February 2022; accepted manuscript online 25 February 2022)

The core structure, Peierls stress and core energy, etc. are comprehensively investigated for the 90° dislocation and the 60° dislocation in metal aluminum using the fully discrete Peierls model, and in particular thermal effects are included for temperature range $0 \leq T \leq 900$ K. For the 90° dislocation, the core clearly dissociates into two partial dislocations with the separating distance $D \sim 12$ Å, and the Peierls stress is very small $\sigma_p < 1$ kPa. The nearly vanishing Peierls stress results from the large characteristic width and a small step length of the 90° dislocation. The 60° dislocation dissociates into 30° and 90° partial dislocations with the separating distance $D \sim 11$ Å. The Peierls stress of the 60° dislocation grows up from 1 MPa to 2 MPa as the temperature increases from 0 K to 900 K. Temperature influence on the core structures is weak for both the 90° dislocation and the 60° dislocation. The core structures theoretically predicted at $T = 0$ K are also confirmed by the first principle simulations.

Keywords: dislocation, temperature effect, aluminum

PACS: 61.72.Bb, 61.72.Lk **DOI:** 10.1088/1674-1056/ac587f

1. Introduction

Great efforts have been made to understanding the dislocation core structure and related properties, and much progress has been achieved before.[1–11] In experiment, several experimental techniques such as x-ray and neutron scattering, high-resolution atomic force microscopy, advanced transmission electron microscopy are applied for probing dislocations core structure at the atomic scale.[3–6] This leads to directly imaging dislocation cores with single-atom sensitivity. Polymorphism of dislocation core structures at the atomic scale was predicted with a model and observed with bicrystal experiments and systematic atomic-resolution imaging.[5] The close match of predicted dislocation cores with direct imaging both geometrically and in quantity offers confidence that the modelling approach represents a reliable routine to pinpointing all core configurations for even a given dislocation type at the atomic scale.[5–8] While the core structures of dislocations are usually modeled and predicted from molecular dynamics simulations,[7–11] it is necessary to develop analytical theory adding a new dimension to understanding the properties of dislocations in real materials.

In 1940s, Peierls put forward a famous equation and obtained its exact solution that can reveal the characteristic size of dislocations and predict the strength of materials.[12,13] The equation is generally named as the Peierls equation and the related model is called the Peierls model or the Peierls–Nabarro (P–N) model.[1] In 1970s, Christian and Vitek suggested that the sinusoidal law in the P–N model should be replaced with the generalized stacking fault energy (γ-surface), which can be obtained directly from the interatomic interaction or from the first principle calculation.[14,15] In order to investigate dislocations with both edge and screw components, such as the dissociated dislocations in the face-centered-cubic (fcc) lattice, the original P–N model was extended to be a so-called 2D model in which the slip displacement is described by a two-dimensional vector.[16] If the change in space between two neighboring slip planes is not negligible, the 2D model should be further extended to a 3D model and in the same time the γ surface should be replaced by the γ-energy function (γ-potential).[17] Lejček and Kroupa presented an equation for the screw dislocation with nonplanar 3-fold structure.[18] Based on Green's formula for half-space and conformal mapping, Ngan derived the general n-fold equation for nonplanar structure of the screw dislocation.[19] Wang and Hu found the exact dislocation solution of the n-fold screw dislocation equation.[20] Merwe extended the Peierls–Nabarro theory to study the interface at which the lattice constant changes.[21–23] The P–N model combined with the γ surface has been widely used to investigate dislocations in a variety of materials.[24–29]

The conventional P–N model is characterized by a nonlinear integro-differential equation that is invariant under con-

†Corresponding author. E-mail: sfwang@cqu.edu.cn

© 2022 Chinese Physical Society and IOP Publishing Ltd

tinuous translation transformation. Obviously, the lattice discreteness is not fully incorporated in the conventional P–N model. For instance, the Peierls barrier vanishes in the the continuum theory and thus dislocation as a topology defect can move freely if there is no ad hoc assumption. In order to evaluate the Peierls stress, one has to assume that the continuous envelope of the discrete slip field is always identical with the solution of the Peierls equation. A semidiscrete variational Peierls framework for dislocation core properties was developed early to investigate the narrow core dislocations in Si.[30] The fully discrete peierls equation was initially derived for a two-dimensional triangular lattice model that can be solved exactly.[31] Later, it was found that based on the spectrum analysis the fully discrete Peierls model can be established in a model-independent way.[32–34] The fully discrete Peierls model can accurately predict the core structure and explore dislocation response to the applied external loading.[34–36] In particular, the Peierls stress can be evaluated in a consistent way in the fully discrete Peierls model. Furthermore, the fully discrete Peierls model can reveal the new modes that appear only in the discrete systems. It is shown that when the lattice discreteness is fully considered, the core of a dislocation may further display various structures (polymorphism). Actually, every dislocation in the continuum theory always splits into two different types with different core.[33–37] The polymorphism of dislocation core structures at the atomic scale attracts much attention.[3,4,7,33–38]

Metal aluminum (Al) is widely used in modern engineering. The mechanical properties of aluminum such as plasticity and yield strength are mainly dominated by the core structure of an individual dislocation and the interaction between dislocations, or between dislocation and impurity.[1] Similar to other fcc metals, the most important dislocations in Al are the 90° dislocation, the 60° dislocation and the screw dislocation. These dislocations dissociate into two partial dislocations with a planar core confined to a $\{111\}$ slip plane.[1,7–9,25,26,36,39–48]

The dislocation core and related properties are determined by crystal structure type and material mechanical features. Because mechanical features of a material are dependent on temperature, the core structure and related properties of dislocations are also temperature-dependent. It is significant to investigate what the influence of temperature on the dislocation is and how the dislocation properties change with temperature. The P–N model explicitly establishes the relationship among the dislocation core structure, the Peierls stress, the elastic constants and the generalized stacking fault energy (γ-surface). Therefore, if changes of the elastic constants and the γ-surface with temperature are known, temperature influence on the dislocation core and the Peierls stress can be predicted theoretically from the P–N model. Recently, the elastic constants and γ surface at finite temperature were calculated for Al from the electron density functional theory, and used to study the 90° dislocation in the frame of the analytical P–N model.[29] Using the data presented in Ref. [29], authors investigated the evolution of the core structure and change of the Peierls stress with temperature.[36] It is found that for the screw dislocation there is stability transformation in the core structure as temperature increases, and the Peierls stress at the transformation temperature becomes remarkably smaller. A question naturally arises: what is the temperature influence on the core structures and the Peierls stress of the 90° dislocation and the 60° dislocation? In this paper, temperature effects on the core structure, core energy, and Peierls stress, etc. are comprehensively investigated for the 90° dislocation and the 60° dislocation using the fully discrete Peierls model. Instead of solving the conventional dislocation equation such as Ref. [29] addressed, the time-dependent dislocation equation (Landau equation) is used to study the equilibrium core structure, the structure relaxation, structure stability, and the motion of dislocations under applied stress field. The new method enables us to numerically obtain very accurate solution and precisely determine dislocation properties. The content is organized as follows. In Section 2, a brief introduction of the fully discrete Peierls model is given. In Sections 3 and 4, the core structure and the Peierls stress calculated from the fully discrete Peierls model are presented for the 90° dislocation and the 60° dislocation, respectively, in temperature range $0 \leq T \leq 900$ K. The temperature influence on the dislocation energy is discussed in Section 5. In Section 6, the stress field is evaluated and plotted for each kind of individual dislocation. In Section 7, the theoretical core structures at the $T = 0$ K are verified by the first principle simulation. Finally, we summarize the results.

2. A brief introduction of the fully discrete Peierls model

Dislocations result from locally relative slip (mismatch or disregistry) between two neighboring lattice planes. The two lattice planes involved are usually referred to as the misfit planes. In order to make statement clear and definite, it is helpful to introduce the cut-plane that locates at the middle of two misfit planes and divides the crystal into two parts. The misfit plane above the cut-plane is named as a-plane and the misfit plane below the cut-plane is named as b-plane. The dislocation core structure is characterized by the slip (mismatch or disregistry) field $S_j(\boldsymbol{R})$ that is defined locally as the relative displacement between the a-plane and b-plane. For the straight dislocation, the dependence of two-dimensional lattice vector $\boldsymbol{R}$ degenerates into a function of a single variable l that measures the distance from the dislocation center. In terms of the slip field, the energy functional (energy in a unit length) of a straight dislocation is[33,34,36]

$$U = U_{\mathrm{i}} + U_{\gamma},$$

$$
\begin{aligned}
U_{\rm i} &= \frac{1}{4\lambda^2}\sum_{l=-\infty}^{\infty}[\beta_{\rm s}\rho_{\rm s}^2(l)+\beta_{\rm e}\rho_{\rm e}^2(l)] \\
&\quad -\frac{1}{4\pi\lambda}\sum_{l=-\infty}^{\infty}\sum_{l'=-\infty}^{\infty}[K_{\rm s}\rho_{\rm s}(l)\rho_{\rm s}(l') \\
&\quad +K_{\rm e}\rho_{\rm e}(l)\rho_{\rm e}(l')]\psi^{(0)}\left(|l-l'|+\frac{1}{2}\right), \\
U_{\gamma} &= \sum_{l=-\infty}^{\infty}\gamma(S_{\rm s},S_{\rm e}),
\end{aligned}
\tag{1}
$$

where $S_{\rm s}$ and $S_{\rm e}$ are the screw and edge components of the slip field, respectively, $\rho_{\rm s}(l)=S_{\rm s}(l+1)-S_{\rm s}(l)$ and $\rho_{\rm e}(l)=S_{\rm e}(l+1)-S_{\rm e}(l)$ are the discrete dislocation densities, $\gamma(S_{\rm s},S_{\rm e})$ is the generalized stacking-fault energy (γ-surface), λ is the step length defined by the distance between two neighboring lattice lines paralleled to the dislocation line, $K_{\rm s}$ and $K_{\rm e}$ are energy factors of the screw and edge dislocations,[1] $\beta_{\rm s}$ and $\beta_{\rm e}$ are the contact-interaction constants,[49] $\psi^{(0)}(z)$ is the Polygamma function. Generally, the energy given by $U_{\rm i}$ is called the interaction energy (self energy) of the dislocation, or the elastic energy of the dislocation, and the energy given by U_{γ} is called the misfit energy. In the isotropic approximation, $K_{\rm s}=\mu$ and $K_{\rm e}=\mu/(1-\nu)$, where μ is the shear modulus and ν is Poisson's ratio.

For the fcc metal Al, the most important glide system are composed of $\{111\}$ planes with the spacing $d=a/\sqrt{3}$, where a is the lattice constant. The γ-surface of the $\{111\}$ plane can be well described by the following expression:[15,29]

$$
\begin{aligned}
\gamma(S_x,S_y) &= \gamma_1\left(\cos\frac{4\pi S_y}{\sqrt{3}b}+2\cos\frac{2\pi S_x}{b}\cos\frac{2\pi S_y}{\sqrt{3}b}\right) \\
&\quad +\gamma_2\left(\sin\frac{4\pi S_y}{\sqrt{3}b}-2\cos\frac{2\pi S_x}{b}\sin\frac{2\pi S_y}{\sqrt{3}b}\right) \\
&\quad +\gamma_3\left(\cos\frac{4\pi S_x}{b}+2\cos\frac{2\pi S_x}{b}\cos\frac{6\pi S_y}{\sqrt{3}b}\right),
\end{aligned}
\tag{2}
$$

where $b=a/\sqrt{2}$ is the magnitude of the Burgers vector (primitive vector) given by the distance between two neighboring atoms, γ_1, γ_2 and γ_3 are three constants. In Eq. (2), the slip field is defined in a coordinate system where the most close-packed lattice line on the plane is selected as the x-axis and the $\{111\}$ plane is selected as the xy plane, and the z-axis is perpendicular to the $\{111\}$ plane. The relative displacement S_z does not appear because it is negligible. The physical constants in expression of the energy functional are functions of temperature.[29,36] In Table 1, all these constants are listed for some typical temperatures in the range $0\le T\le 900$ K.

Table 1. The physical constants of metal aluminum.

T (K)	a (Å)	ν	$K_{\rm s}$ (GPa)	γ_1 (J/m^2)	γ_2 (J/m^2)	γ_3 (J/m^2)	$\beta_{\rm s}$ (J/m^2)	$\beta_{\rm e}$ (J/m^2)	$K_{\rm e}$ (GPa)
0	4.053	0.348	28.56	−141.4	−195.2	3.735	4.382	19.61	43.80
100	4.055	0.350	27.89	−140.6	−195.0	3.726	4.285	19.38	42.91
200	4.062	0.352	26.99	−137.4	−190.3	3.693	4.154	19.00	41.65
300	4.071	0.355	25.69	−133.4	−184.5	3.691	3.963	18.45	39.83
400	4.081	0.358	24.28	−129.1	−178.2	3.689	3.754	17.79	37.82
500	4.091	0.363	22.75	−124.4	−171.4	3.683	3.526	17.23	35.71
600	4.103	0.367	21.23	−119.5	−164.3	3.675	3.300	16.54	33.54
700	4.116	0.372	19.69	−114.9	−157.8	3.777	3.071	15.90	31.35
800	4.129	0.377	18.02	−109.5	−150.1	3.732	2.819	15.11	28.92
900	4.144	0.385	16.15	−104.0	−142.4	3.493	2.536	14.41	26.26

For the 90° dislocation shown in Fig. 1, the dislocation line is along the $\langle\bar{1}\bar{1}2\rangle$ direction, the Burgers vector is $\boldsymbol{b}=\frac{1}{2}\langle\bar{1}10\rangle$, and thus $S_{\rm s}=S_y$ and $S_{\rm e}=S_x$. The boundary conditions of the slip field are

$$
S_{\rm e}(\infty)-S_{\rm e}(-\infty)=b,\quad S_{\rm s}(\infty)-S_{\rm s}(-\infty)=0.
$$

For the 60° dislocation shown in Fig. 2, the dislocation line is along the $\langle\bar{1}10\rangle$, the Burgers vector is $\boldsymbol{b}=\frac{1}{2}\langle\bar{1}01\rangle$, and thus $S_{\rm s}=S_x$, $S_{\rm e}=S_y$, the boundary conditions are

$$
S_{\rm e}(\infty)-S_{\rm e}(-\infty)=\frac{\sqrt{3}b}{2},\quad S_{\rm s}(\infty)-S_{\rm s}(-\infty)=\frac{b}{2}.
$$

For the screw dislocation, $S_{\rm s}=S_x$, $S_{\rm e}=S_y$, the boundary conditions are

$$
S_{\rm s}(\infty)-S_{\rm s}(-\infty)=b,\quad S_{\rm e}(\infty)-S_{\rm e}(-\infty)=0.
$$

The core structure of a free dislocation is determined by the minimum energy principle. However, if there is external stress $\sigma^0=(\sigma_{\rm s}^0,\sigma_{\rm e}^0)$ (resolved shear stress on the $\{111\}$ plane), we should introduce the Gibbs energy

$$
G=U-\sum_{l=-\infty}^{\infty}(\sigma_{\rm s}^0S_{\rm s}+\sigma_{\rm e}^0S_{\rm e}),
\tag{3}
$$

and the dislocation equation satisfied by the slip field is given by the following variational principle

$$
\frac{\delta G}{\delta S_{\rm s}}=0,\quad \frac{\delta G}{\delta S_{\rm e}}=0.
$$

In order to study the structure relaxation, structure stability, and the motion of dislocations under applied stress field, we propose to introduce the time-dependent dislocation equation (Landau equation)

$$
\Gamma\frac{\partial S_{\rm s}}{\partial t}=-\frac{\delta G}{\delta S_{\rm s}},\quad \Gamma\frac{\partial S_{\rm e}}{\partial t}=-\frac{\delta G}{\delta S_{\rm e}},
\tag{4}
$$

where Γ is the effective damping constant. For mechanical processes there is a characteristic time, $t_c = a/c_t$, a ratio between the lattice constant a and the transverse wave velocity c_t. It is rational to take the damping time in the same order with the characteristic time

$$\Gamma \sim \frac{2\pi}{t_c} \times \frac{\mu}{a},$$

where $\mu = K_s$ is the shear modulus. The exact value of the damping constant is of no great importance for the results obtained in this study. In the following, similar to the phase field theory of dislocations,[50] the time-dependent Landau equation is employed to obtain the equilibrium core and to determine the Peierls stress. As an efficient way, the stable equilibrium slip field can be obtained by relaxing an input solution with the asymptotic behavior given by the Peierls solution (boundary condition).[12,33] After the stable equilibrium slip field is obtained, the external stress field is applied gradually to explore how the dislocation responds. The Peierls stress is the critical stress at which the dislocation starts moving.

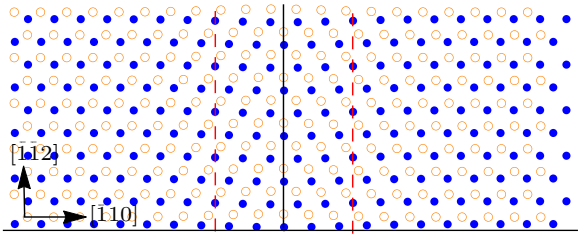


Fig. 1. The atomic configurations of the dissociated 90° dislocation at $T = 0$ K, where the empty circles and solid circles represent the atoms on the a-plane (above the cut plane) and the b-plane (below the cut plane), respectively. The symmetric-center line is marked by the solid line and the partial dislocations are marked by the dashed lines.

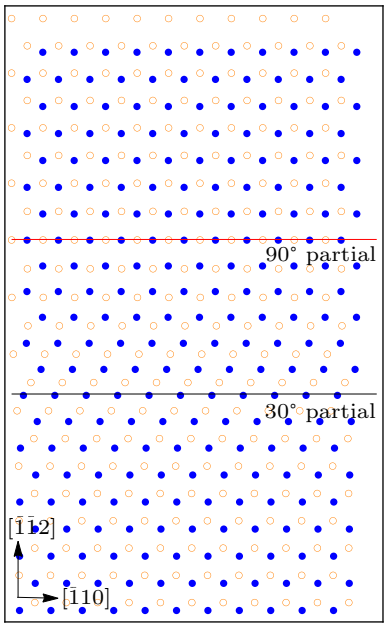


Fig. 2. The atom configuration on the a-plane (solid circles) and b-plane (empty circles) for the 60° dislocation) at $T = 0$ K. The 60° dislocation clearly dissociates into 30° and 90° partial dislocations separated by a small stacking fault band. The center of each partial dislocation is marked with a solid line.

3. The 90° dislocation

The 90° dislocation is the $\frac{1}{2}\langle 110\rangle\{111\}$ edge dislocation. The Burgers vector is $b = a/\sqrt{2}$, and the step length is $\lambda = a/(2\sqrt{2}) \approx 0.35a$. There are two different equilibrium cores. One is the compact core that has no stacking fault band and no screw slip component $S_s = 0$. The other is the splitting core that has stacking fault band separating two partial dislocations, and the local screw slip component is not zero, $S_s \neq 0$. It is found that even though the compact Peierls solution is input as the initial condition of the time-dependent dislocation equation (4), the dislocation always spontaneously evolves into the splitting core. The results indicate that the compact core is unstable. In the following, we focus on the stable splitting core. The atomic configurations ($T = 0$ K) resulting from the stable solution to Eq. (4) is plotted in Fig. 1. Obviously, there is a stacking fault band separating two partial dislocations. In Fig. 3, the slip field (S_e, S_s) and the density distribution (ρ_e, ρ_s) at $T = 0$ K are shown. From the density distribution of the edge component, we see that the 90° dislocation symmetrically dissociates into two partial dislocations. The separate distance is $D = 12.8$ Å (the distance between the two peaks), which agrees with data 10.3 Å obtained from the Peierls–Nabarro model[42] and 15 Å obtained from molecular dynamics (MD).[51] As a edge dislocation, the screw component of the 90° dislocation is induced by the edge slip and the total sum of the screw component is zero. However, as shown in Fig. 3, the amplitude of the screw component is comparable to that of the edge component. The screw component can be viewed as a pair of dislocation and anti-dislocation.

The shear stress produced by the dislocation on the misfit plane (a-plane or b-plane) is evaluated and the results are shown in Fig. 4. The shear stress (σ_x) in the (edge) direction perpendicular to the dislocation line is nearly double of that (σ_y) along the (screw) parallel direction. At the positions of the partial dislocations the shear stress σ_x has its maximum $0.1\mu \approx 3$ GPa. At the center of the dislocation, the shear stress σ_y has the maximum $0.05\mu \approx 1.5$ GPa. To examine the accuracy, the shear stress originated from the γ-surface is also evaluated. As shown in Fig. 4, two forces perfectly balance each other in our calculations. This implies that the solution obtained is very accurate.

The slip field and the density are plotted in Fig. 5 for temperatures $T = 0$ K, 500 K, 800 K, 900 K. It is observed that the slip field and the related density change little as temperature increases. For the edge dislocation, temperature effect on the core structure is so weak that it can be neglected safely.

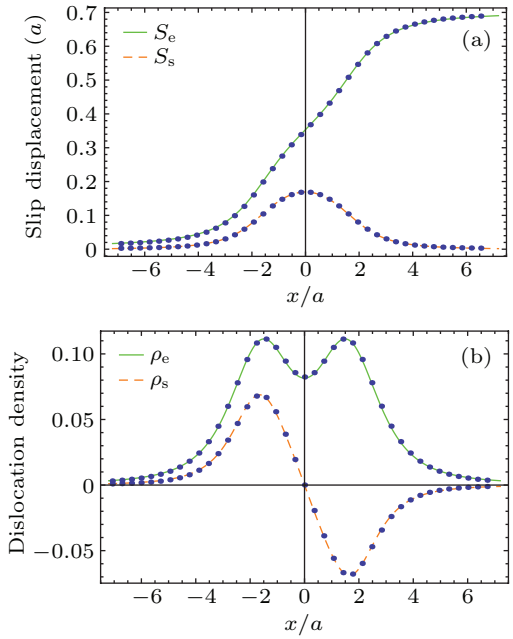


Fig. 3. The slip field (a) and the dislocation density (b) of the 90° dislocation at $T = 0$ K. The edge component clearly splits into two partial dislocations (peaks) while the screw component shows feature of dislocation dipole. The calculated data (scatter points) can be well fitted by superpositions of dislocations [solid and dashed lines given by fitting Eqs. (6) and (7)].

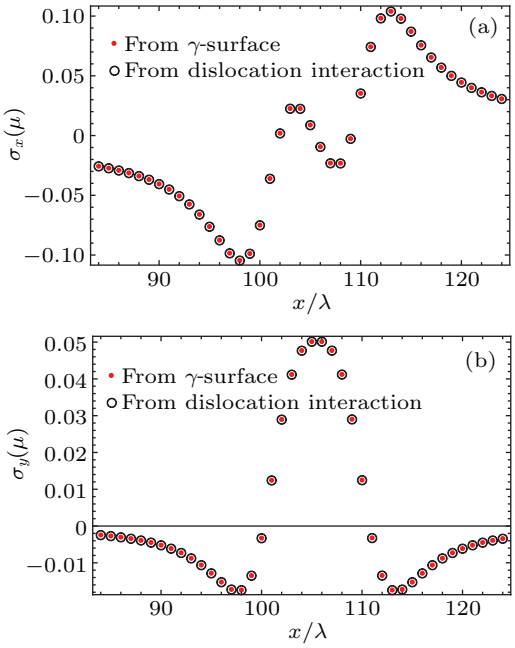


Fig. 4. The shear stress (empty circles in (a) and (b)) produced by the infinitesimal dislocation distribution on the misfit plane at $T = 0$ K. The stress is precisely balanced by that resulting from the γ-surface (solid circles). The result indicates that the solution obtained is very accurate.

It is useful to obtain an analytical expression for the numerical slip field solution. In order to obtain an analytical expression, we introduce the standard slip field

$$S^{(0)}(x,c) = \frac{b}{2\pi}\left(\arctan\frac{x}{\zeta} + \frac{c\zeta x}{\zeta^2 + x^2}\right), \quad \zeta = \frac{\zeta_p}{1-c}, \tag{5}$$

where c is a parameter that describes the core structure, ζ is the characteristic length that can be viewed as the core width, ζ_p is the Peierls width ($\zeta_p = d/2$ for the screw slip and $\zeta_p = d/2(1-\nu)$ for the edge slip, $d = a/\sqrt{3}$ is the spacing of the $\{111\}$ planes). The the standard slip field represents a half-dislocation because the Burgers vector of the standard slip field is

$$S^{(0)}(\infty,c) - S^{(0)}(-\infty,c) = \frac{b}{2}.$$

In the following, we will see that the complex core can be viewed as a superposition of several standard slip fields with different core parameters.

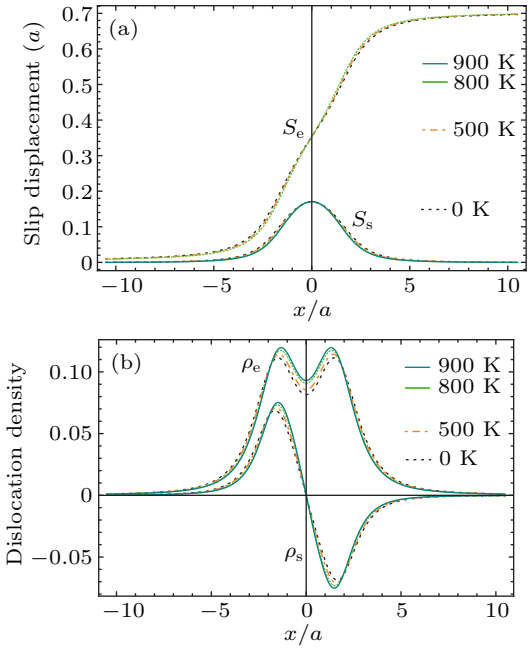


Fig. 5. The slip field (a) and the dislocation density (b) along the Burgers vector direction at temperatures $T = 0$ K, 500 K, 800 K, 900 K.

The edge component (slip component perpendicular to the dislocation line) of the numerical solution of the 90° dislocation can be well described by superposition of two partial dislocations:

$$\begin{aligned} &S_e(x) = S^{(0)}\left(x - \frac{D_e}{2}, c\right) + S^{(0)}\left(x + \frac{D_e}{2}, c\right) + \frac{b}{2}, \\ &x = \ell\lambda, \end{aligned} \tag{6}$$

with c and D_e being the parameters determined by fitting. The screw component can be well described by superposition of two dislocation dipoles:

$$\begin{aligned} &S_s(x) = \sum_{i=1}^{2}\frac{1}{2}\left[S^{(0)}\left(x - \frac{D_s}{2}, c_i\right) - S^{(0)}\left(x + \frac{D_s}{2}, c_i\right)\right], \\ &\zeta_i = \frac{\zeta_p}{1-c_i}. \end{aligned} \tag{7}$$

In Table 2, the parameters c, ζ, c_1, c_2, ζ_1, ζ_2 and the separation distances D_e, D_s are listed for various temperature. The largest effect of the temperature on the core structure focuses on the separation distance D that decreases with increasing temperature.

Table 2. The parameters in the fitting solutions of the edge dislocation.

T (K)	c	ζ (Å)	D_e (Å)	c_1	c_2	ζ_1 (Å)	ζ_2 (Å)	D_s (Å)
0	0.784	8.105	12.838	0.824	0.741	9.950	6.762	13.371
100	0.786	8.066	12.929	0.827	0.743	9.971	6.710	13.450
200	0.787	8.077	12.878	0.826	0.744	9.922	6.718	13.397
300	0.788	8.067	12.762	0.826	0.745	9.813	6.710	13.277
400	0.790	8.052	12.617	0.825	0.748	9.682	6.696	13.127
500	0.793	8.049	12.484	0.825	0.750	9.544	6.687	12.985
600	0.795	8.038	12.330	0.825	0.753	9.399	6.675	12.824
700	0.798	8.041	12.214	0.825	0.757	9.264	6.677	12.696
800	0.801	8.005	12.026	0.825	0.761	9.077	6.638	12.495
900	0.807	7.920	11.824	0.827	0.766	8.844	6.526	12.266

In the fully discrete Peierls model, the Peierls stress σ_p can be naturally evaluated without any ad hoc assumption. Applying an external stress σ_0 gradually, we can obtain the critical stress $\sigma_0 = \sigma_p$, at which the dislocation starts moving through crystal. For the 90° dislocation, we find that the Peierls stress is so small that can hardly be observed in the numerical calculation. The upper limit is about $\sigma_p < 10^{-8}\mu \sim 1$ kPa. Such a small upper limit indicates that the Peierls stress nearly vanishes for the 90° dislocation.

In the original P–N model, the width of an edge dislocation and the Peierls stress are given as follows:

$$\zeta_p = \frac{d}{2(1-\nu)}, \quad \sigma_p = \frac{\mu}{1-\nu} e^{-\frac{\pi d}{(1-\nu)b}}.$$

Taking $\mu = 28.56$ GPa, $\nu = 0.348$, $a = 4.053$ Å, $b = a/\sqrt{2}$, $d = a/\sqrt{3}$ for $T = 0$ K, we have

$$\zeta_p \approx 1.8 \text{ Å}, \quad \sigma_p \approx 0.03\mu \sim 800 \text{ MPa}.$$

Apparently, the results given in the original P–N model cannot be simply applied for the 90° dislocation in Al. It is instructive to express the Peierls stress in the term of the width

$$\sigma_p = K e^{-\frac{2\pi\zeta}{b}},$$

where K is the energy factor, $K = \frac{\mu}{1-\nu}$ for the edge dislocation, $K = \mu$ for the screw dislocation. Noting that the Burgers vector b is the characteristic length (period) of the discrete lattice in the original P–N model, this expression indicates that the Peierls stress results from competition between the dislocation width ζ and the discrete length b. This explanation gives a key insight into the Peierls stress. However, if the Burgers vector b is not the lattice period in the dislocation moving direction, it must be further elucidated. Generally, the discrete length b should be interpreted as the step length λ that is the period of the misfit plane along the dislocation moving direction. For a dislocation, if the step length is much smaller than the width, $\lambda \ll \zeta$, the dislocation will feel little discreteness and the Peierls stress will be very small no matter how large the Burgers vector (minimum lattice vector) is. Therefore, the the Peierls stress formula should be modified as follows:[52]

$$\sigma_p = K e^{-\frac{2\pi\zeta}{\lambda}}, \tag{8}$$

i.e., the Peierls stress results from competition between the dislocation width ζ and the step length λ. For the 90° dislocation, it is reasonable to identify the width ζ with that appearing in the standard slip field Eq. (5). For $T = 0$ K, we have $\zeta \sim 7$ Å, $\lambda \sim 1.4$ Å, and $\sigma_p \sim 10^{-13}\mu$. The Peierls stress is nearly zero for the 90° dislocation indeed. This estimation qualitatively explains why the Peierls stress is so small for the 90° dislocation.

4. The 60° dislocation

The Burgers vector for the 60° dislocation is the same in magnitude as that of the 90° dislocation, $b = a/\sqrt{2}$. However, the step length is almost double of that of the 90° dislocation, $\lambda = \sqrt{6}a/4 = 0.61a$. The 60° dislocation is a mixed dislocation. For the mixed dislocation, instead of the natural frame in which the slip vector is decomposed into the edge and screw components, it is more convenient to use the intrinsic frame in which one axis is given by Burger's vector.[53] In the intrinsic frame, the slip vector is decomposed into $\boldsymbol{S} = \boldsymbol{S}_\parallel + \boldsymbol{S}_\perp$, where $\boldsymbol{S}_\parallel$ is the component along Burger's vector and $\boldsymbol{S}_\perp$ is the component perpendicular to Burger's vector. The transformation relationship between the components in the natural frame and the intrinsic frame is[53]

$$\begin{pmatrix} S_\parallel \\ S_\perp \end{pmatrix} = \begin{pmatrix} \sin\phi & \cos\phi \\ -\cos\phi & \sin\phi \end{pmatrix} \begin{pmatrix} S_e \\ S_s \end{pmatrix}, \tag{9}$$

where $\phi = 60°$ is the angle between the dislocation line and Burger's vector.

Replacing the edge and screw components (S_e, S_s) in the evolution equation (4) by the parallel and perpendicular components $(S_\parallel, S_\perp)$, we have the equation satisfied by the components $(S_\parallel, S_\perp)$. Similarly, the stable dislocation solution of the equation can be automatically obtained by relaxing an input solution with the boundary condition

$$S_\parallel(\infty) - S_\parallel(-\infty) = b, \quad S_\perp(\infty) - S_\perp(-\infty) = 0.$$

The slip field components $S_\parallel$ and $S_\perp$ are firstly evaluated at temperature $T = 0$ K for the 60° dislocation. In Figs. 6 and 7, the slip field components in both the natural and intrinsic frame are plotted. We see that the density distribution of the screw component is compact while the density distribution of the edge component obviously dissociates into two parts. In Fig. 2, the atom configuration on the a-plane (solid circles) and the b-plane (empty circles) are explicitly plotted based on the slip field obtained. Apparently, the 60° dislocation clearly dissociates into 30° and 90° partial dislocations separated by a small stacking fault band.

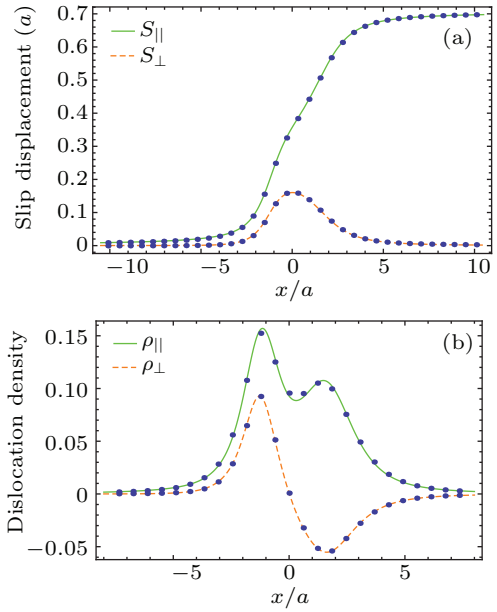


Fig. 6. The fitting results of the numerical solution (scattered points) at $T = 0$ K. The solid and dashed lines are from the fitting equations (10) and (12). From the density distribution (b), it can be seen that the 60° dislocation splits into two asymmetric parts.

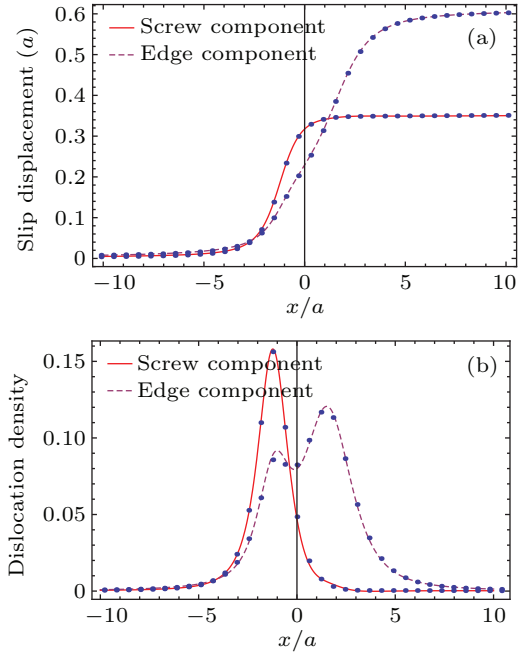


Fig. 7. The slip field and density distribution of the edge component and screw component in the natural frame at $T = 0$ K. From the density distribution (b), it can be seen that the screw component of 60° dislocation is compact while the edge component dissociates obviously.

The shear stress produced by the dislocation on the misfit plane (a-plane or b-plane) is shown in Fig. 8 for $T = 0$ K. The stress distribution of the 60° dislocation is not symmetric. Similar to the 90° dislocation, the major shear stress results from the parallel slip (parallel to Burgers vector). The maximum shear stress is about $0.1\mu \approx 3$ GPa that locates at the centers of the partial dislocations. The normal shear stress (perpendicular to Burgers vector) is about $0.6\mu \approx 1.8$ GPa. To verify the accuracy of the solution, the stress that originates from the γ-surface is also evaluated. As seen in Fig. 8, the shear stress produced by the dislocation is precisely balanced by that from the γ-surface.

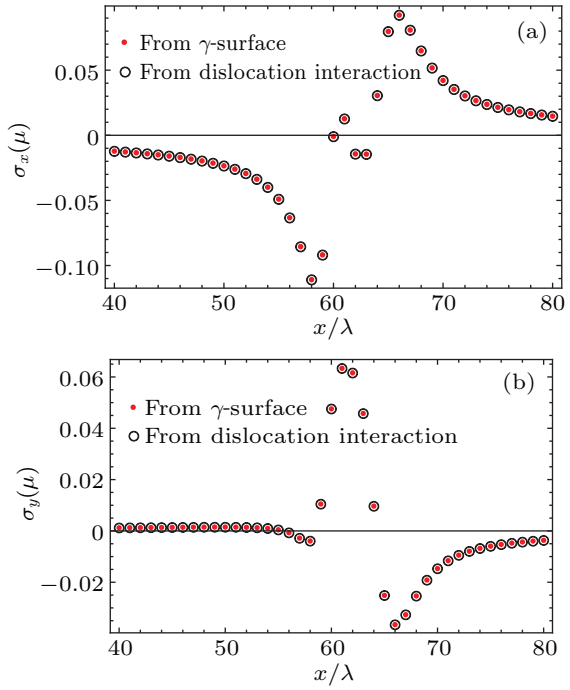


Fig. 8. For the numerical solution of 60° dislocation at $T = 0$ K, the stress resulting from the γ-surface (solid circles) is precisely balanced by the stress resulting from the distribution of infinitesimal interactions (empty circles).

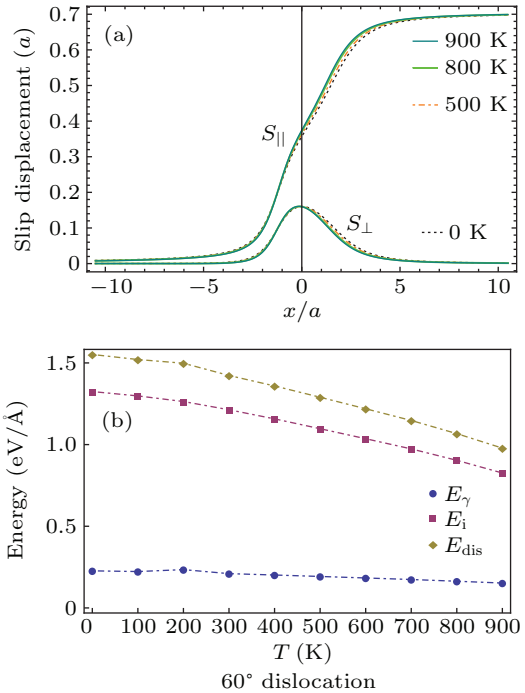


Fig. 9. The slip field (a) and the dislocation energy (b) at temperatures $T = 0$ K, 500 K, 800 K, 900 K.

The slip field and the density are plotted in Fig. 9 for temperatures $T = 0$ K, 500 K, 800 K, 900 K. It is observed that similar to the edge dislocation the slip field and the related density change little as temperature increases. In Fig. 10, the Peierls stress σ_{p} is plotted as a function of temperature.

Surprisingly, the Peierls stress grows up monotonically from 1 MPa to 2 MPa as temperature increases from 0 K to 900 K. The order of the Peierls stress is same as the yield strength of Al observed in experiment.[54] The Peierls stress can also be estimated from Eq. (8). If the characteristic width is chosen to the smallest one $\zeta = 4.735$ Å and $\zeta = 4.271$ Å (Table 5), respectively, for $T = 0$ K and $T = 900$, the Peierls stresses from Eq. (8) are $\sigma_{\rm p} = 0.17$ MPa and $\sigma_{\rm p} = 0.4$ MPa. The values are one order smaller than that obtained in our discrete model, but the increasing tendency with temperature is same.

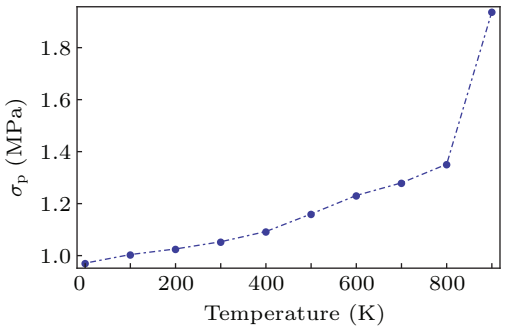


Fig. 10. The Peierls stress as a function of temperature for the 60° dislocation.

For the 60° dislocation, the parallel slip component $S_{\parallel}$ of the numerical solutions can be well described by superposition of two partial dislocations:

$$S_{\parallel}(x) = S^{(0)}(x - x_1, c_1) + S^{(0)}(x - x_2, c_2) + \frac{b}{2}, \qquad (10)$$

where

$$\zeta_i = \frac{d}{2(1-\tilde{\nu})(1-c_i)},$$
$$1 - \tilde{\nu} = \frac{1-\nu}{(1-\nu)\cos^2\phi + \sin^2\phi}, \quad i = 1, 2. \qquad (11)$$

The fitting parameters are listed in Table 3.

The normal slip component can also be described by superposition of partial dislocations and anti-dislocations:

$$S_{\perp}(x) = \sum_{i=1}^{2} \frac{1}{2}[S^{(0)}(x - x_i', c_i') - S^{(0)}(x - x_i'', c_i'')], \qquad (12)$$

Due to the asymmetric core of 60° dislocation, we need superposition of four partial dislocations (two partial dislocations plus two partial anti-dislocation) to fit the data. The fitting parameters are listed in Table 4. Figure 6 shows the fitting results of the numerical solution at $T = 0$ K. The analytical expression is well coincided with the numerical solution. The two peaks in the dislocation density implies dissociation of the 60° dislocation. The dissociation distance is $D \approx 11$ Å. This value is slightly smaller than that (13 Å) of the 90° dislocation, but much larger than that (4 Å) of the screw dislocation.[36] The splitting width obtained by atomistic simulation is ~ 10 Å.[55] From Tables 3 and 5, we see that the widths of partial dislocations slowly decrease as temperature increases. That is why the Peierls stress grows up with temperature.

Table 3. The fitting parameters for the parallel component of the slip field.

T (K)	c_1	c_2	x_1 (a)	x_2 (a)	ζ_1 (Å)	ζ_2 (Å)	D (Å)
0	0.710	0.810	–1.192	1.580	5.506	8.415	11.238
100	0.712	0.812	–1.192	1.598	5.465	8.375	11.313
200	0.712	0.813	–1.193	1.580	5.456	8.387	11.263
300	0.713	0.814	–1.193	1.546	5.425	8.378	11.154
400	0.714	0.816	–1.194	1.506	5.387	8.360	11.020
500	0.716	0.818	–1.195	1.467	5.343	8.358	10.892
600	0.718	0.821	–1.196	1.424	5.299	8.345	10.749
700	0.720	0.824	–1.197	1.387	5.257	8.349	10.638
800	0.722	0.827	–1.199	1.336	5.186	8.310	10.465
900	0.727	0.832	–1.199	1.280	5.054	8.218	10.274

Table 4. The fitting parameters for the normal component of the slip field.

T (K)	c_1'	c_2'	c_1''	c_2''	x_1' (a)	x_2' (a)	x_1'' (a)	x_2'' (a)
0	0.663	0.813	0.815	0.872	–1.258	–0.955	1.630	–0.137
100	0.664	0.814	0.817	0.873	–1.259	–0.951	1.649	–0.144
200	0.664	0.814	0.818	0.873	–1.259	–0.956	1.631	–0.149
300	0.665	0.814	0.820	0.873	–1.259	–0.963	1.595	–0.161
400	0.666	0.813	0.822	0.873	–1.259	–0.972	1.553	–0.173
500	0.668	0.813	0.825	0.874	–1.260	–0.981	1.511	–0.189
600	0.670	0.813	0.827	0.874	–1.260	–0.991	1.465	–0.203
700	0.672	0.813	0.831	0.875	–1.261	–1.001	1.427	–0.217
800	0.675	0.813	0.834	0.876	–1.262	–1.010	1.373	–0.237
900	0.677	0.815	0.840	0.878	–1.262	–1.016	1.316	–0.268

Table 5. The core widths and the separating distances of the partial dislocations.

T (K)	ζ_1' (Å)	ζ_2' (Å)	ζ_1'' (Å)	ζ_2'' (Å)	D (Å)
0	4.735	8.528	8.646	12.430	11.742
100	4.684	8.492	8.598	12.398	11.803
200	4.676	8.448	8.621	12.361	11.750
300	4.648	8.356	8.630	12.264	11.634
400	4.613	8.251	8.631	12.146	11.493
500	4.570	8.119	8.654	12.019	11.352
600	4.530	7.995	8.666	11.885	11.198
700	4.493	7.861	8.698	11.753	11.072
800	4.422	7.695	8.687	11.563	10.880
900	4.271	7.452	8.623	11.280	10.654

5. The self-energy and the misfit energy

In theory, the dislocation energy consists of the interaction energy (self energy) of the infinitesimal dislocations and the misfit energy. The self energy and the misfit energy can be straightforwardly evaluated from the functional $U_{\rm i}$ and U_{γ} in Eq. (1) when the solution of the slip field is obtained. In Fig. 11, as a function of temperature, the self energy $E_{\rm i}$ and the misfit energy E_{γ} are shown for the 90° dislocation, the 60° dislocation and the screw dislocation, respectively. The self energy $E_{\rm i}$ falls off as temperature increase while the misfit energy E_{γ} has a peak at temperature $T \sim 200$ K. In evaluation of the self energy, the logarithmic divergence is removed by truncating the summation of the long range interaction to the range $-52b \le \ell\lambda \le 52b$.

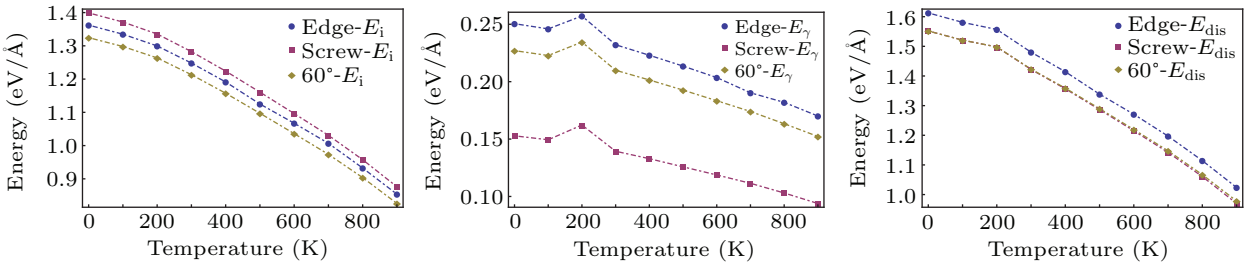


Fig. 11. The self energy E_i, the misfit energy E_γ, and the dislocation core energy $E_{dis} = E_i + E_\gamma$ for the 90° (edge) dislocation, the 60° dislocation, and the screw dislocation.

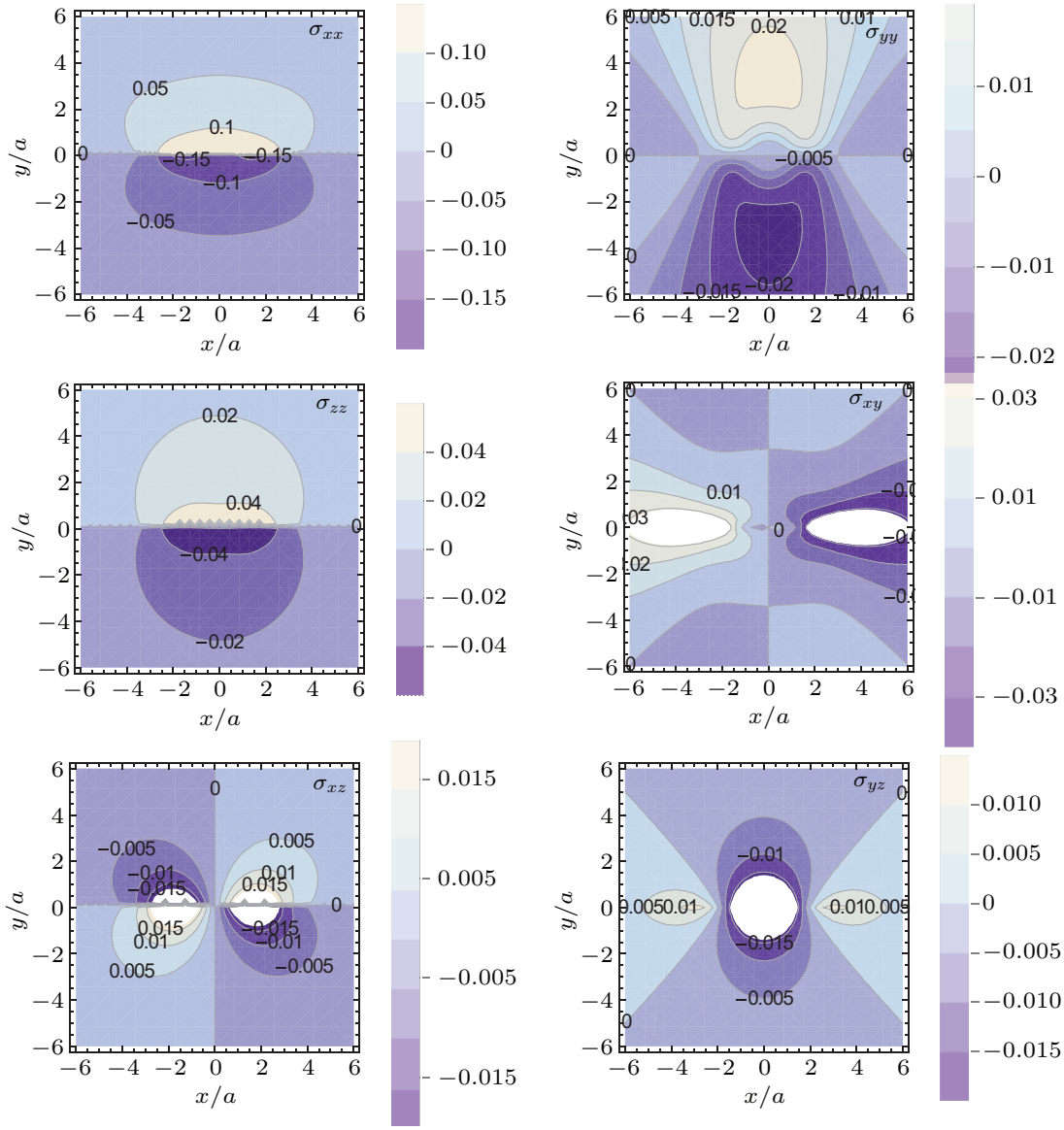


Fig. 12. The stress field on the plane perpendicular to the 90° dislocation line (z-axis). The stress is measured by the shear modulus μ and the length is measured by the lattice constant a. The x-axis is chosen to be parallel to the Burgers vector.

6. The stress field

In this section, we calculate the stress field and the displacement field in the isotropic approximation. It should be emphasized that the coordinates system chosen in this section is the same as that utilized usually in the continuum theory of dislocations, but different from that used in the previous section. Specifically, the coordinates system is chosen so that the z-axis is parallel to the dislocation line, the xz plane is the glide plane (the $\{111\}$ plane) and the normal of the glide plane is the y-axis.

For an edge dislocation described by the standard slip field

$$S^{(0)}(x,c) = \frac{b}{2\pi}\left(\arctan\frac{x}{\zeta} + \frac{c\zeta x}{\zeta^2 + x^2}\right), \tag{13}$$

the stress function is[34]

$$\psi_x^{(0)}(x,y) = \frac{b\mu y}{8\pi(1-\nu)}\left\{\ln[x^2+(|y|+\zeta)^2] - \frac{2c\zeta(|y|+\zeta)}{x^2+(|y|+\zeta)^2}\right\}. \quad (14)$$

For a screw dislocation with the standard slip field, it can be shown that apart from a constant the displacement field is simply given by replacing $\zeta \to \zeta + |y|$ in Eq. (13),

$$u_z = \frac{b}{2\pi}\left[\left(\arctan\frac{x}{|y|+\zeta}\right) + \frac{c\zeta x}{x^2+(|y|+\zeta)^2}\right] + u_z^{(0)}. \quad (15)$$

In addition, for a edge slip field of dislocation dipole

$$S_e(x) = \frac{c\zeta^2}{\zeta^2+x^2},$$

it is easy to know that the stress function is

$$\psi_e(x,y) = \frac{\mu\zeta cxy}{2(1-\nu)[x^2+(|y|+\zeta)^2]}. \quad (16)$$

Obviously, for the slip fields given in superposition of the basic slip $S^{(0)}$, the related fields can be obtained by the superposition principle. Therefore, from Eqs. (14)–(16), using the superposition principle, the stress field and the displacement can be explicitly evaluated for each individual dislocation discussed above.[34,56,57] The analytical expressions of the stress fields are very complex and omitted here. In Figs. 12–14, the stress fields are plotted for the 90° dislocation, the 60° dislocation and the screw dislocation respectively.

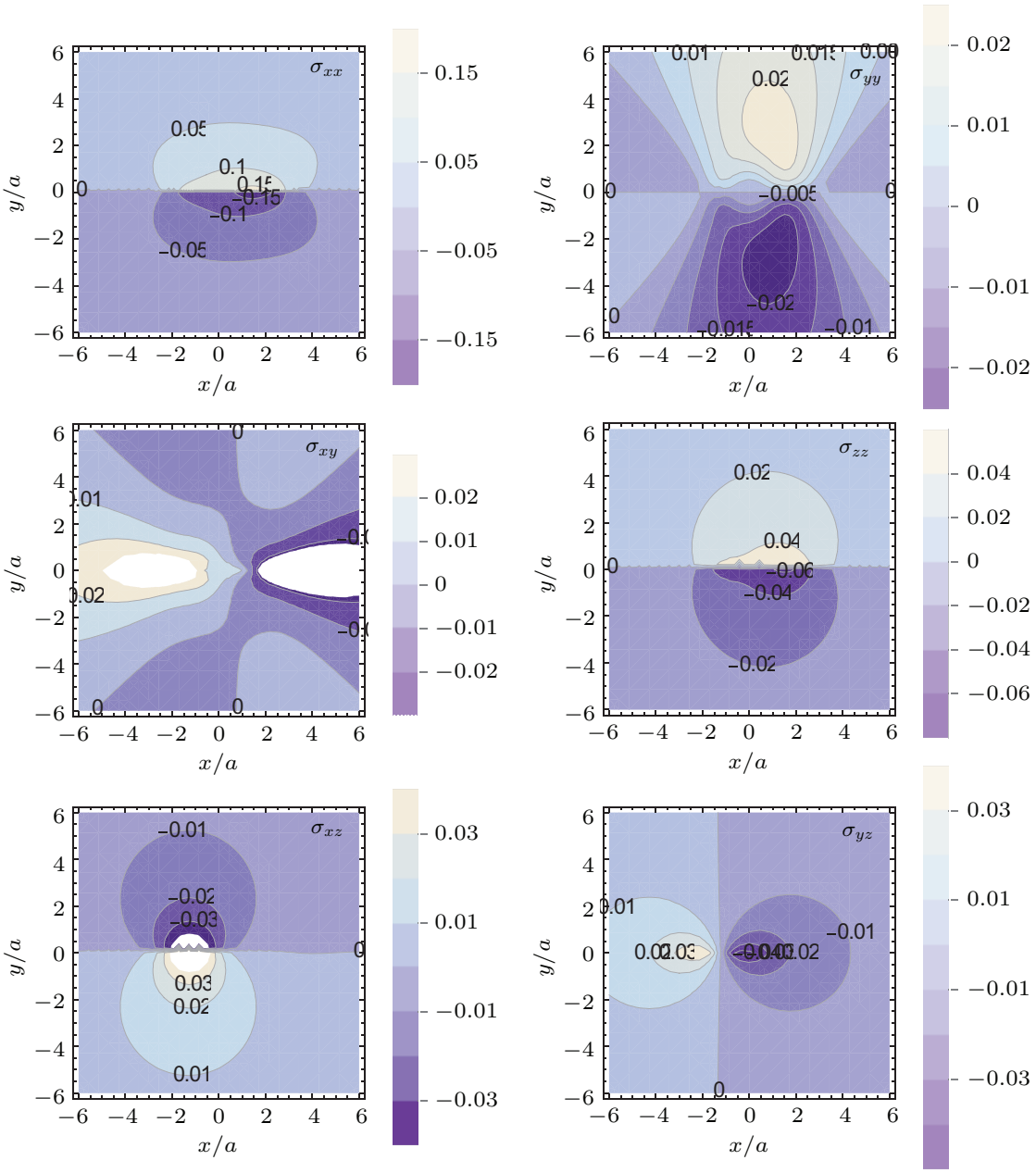


Fig. 13. The stress field on the plane perpendicular to the 60° dislocation line (z-axis). The stress is measured by the shear modulus μ and the length is measured by the lattice constant a. The x-axis is chosen to be parallel to the edge component of Burgers vector.

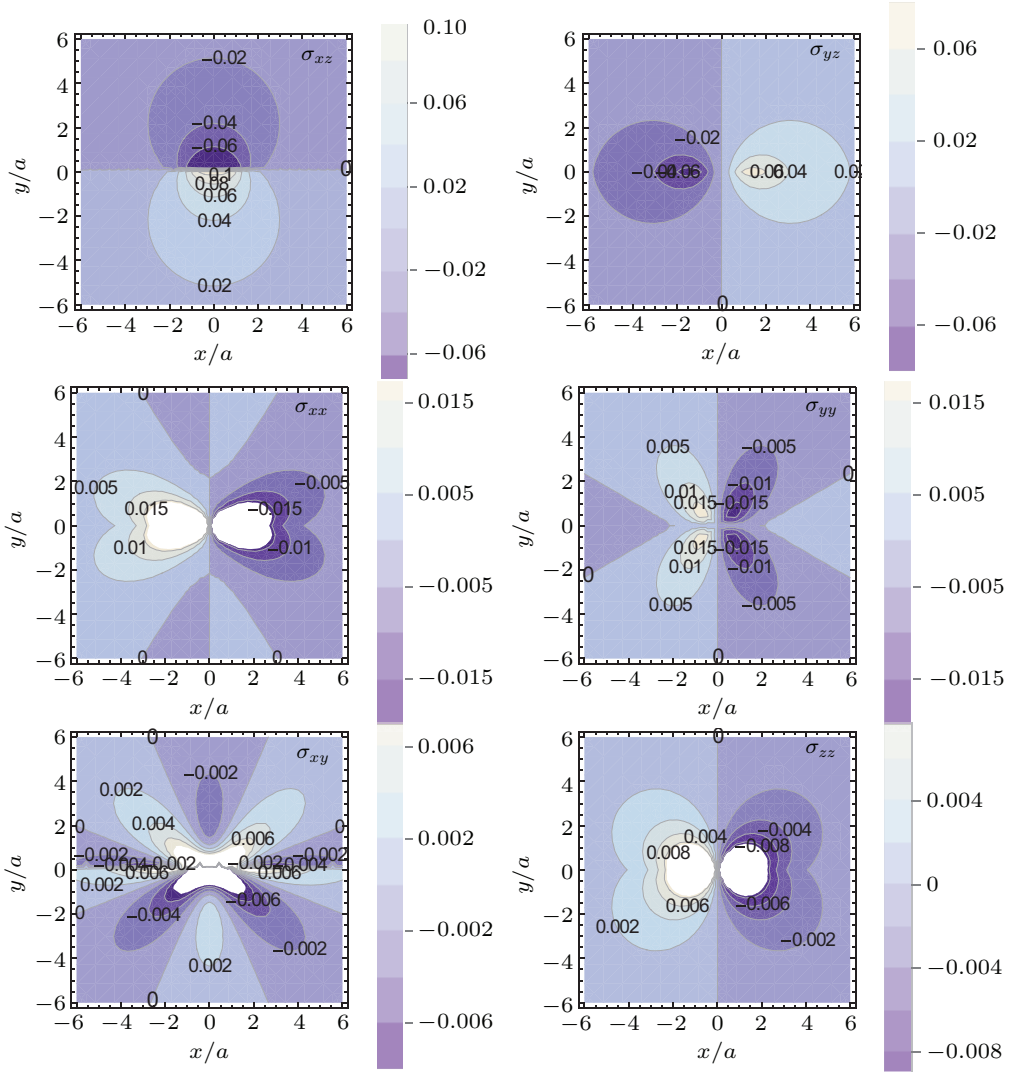


Fig. 14. The stress field on the plane perpendicular to the screw dislocation line (z-axis). The stress is measured by the shear modulus μ and the length is measured by the lattice constant a. The slip field used is taken from Ref. [36].

7. The dislocation cores from the first principle calculations

As is well known, the long range feature of the dislocations makes it difficult to simulate the dislocation precisely. Usually, the periodic array of dislocation dipoles is used in dislocation simulations. However, when the long range problem is overcome for the array of dislocation dipoles, the interaction between the dislocation and anti-dislocation is introduced. The interaction between the dislocations falls off inversely proportional to the distance, and is not small for the small periodic cell.

It is efficient to simulate the dislocation core with help of analytical predictions because the dislocation core actually involves a few atoms around the center of the dislocation and the far field can be precisely obtained in the elastic theory. We suggest to simulate dislocation in the electron density functional theory using the shelled cell given by a pre-calculation carried out in the fully discrete Peierls theory. The shelled cell contains an isolated dislocation with a rigid shell in which the atom positions are given by the theory prediction. As long as the thickness of the shell is larger than the characteristic length of the interaction range, the surface effects are negligible and the relaxation will take place only at the core, and thus an accurate dislocation core can be obtained from the first principle simulation.

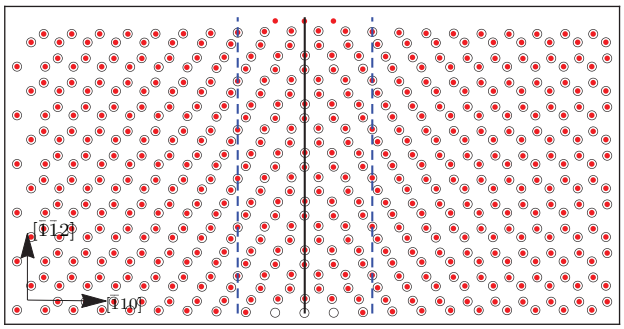


Fig. 15. The atom alignments on the a-plane and b-plane of the edge dislocation given by the theory (big empty circles) and the first-principles calculation (small solid circles). There are 252 atoms in the super-cell used. The initial total energy is -902.215 eV and the final energy is -902.447 eV. Theoretical prediction is confirmed satisfactorily.

In order to confirm the theoretical predictions, the 90°, 60° and screw dislocation cores are relaxed by using the Vienna *ab initio* simulation package (VASP) developed at the Institut fur Materialphysik of Universitat Wien.[58–60] The Perdew–Burke–Ernzernhof exchange-correlation functional for the generalized gradient-approximation is used in our calculations. A plane wave basis is employed within the framework of the projector augmented wave method. The structure is relaxed with a plane-wave energy cutoff of 450 eV. The iteration convergence is chosen to be 10^{-4} eV and 10^{-3} eV/Å for the energy and the force respectively.

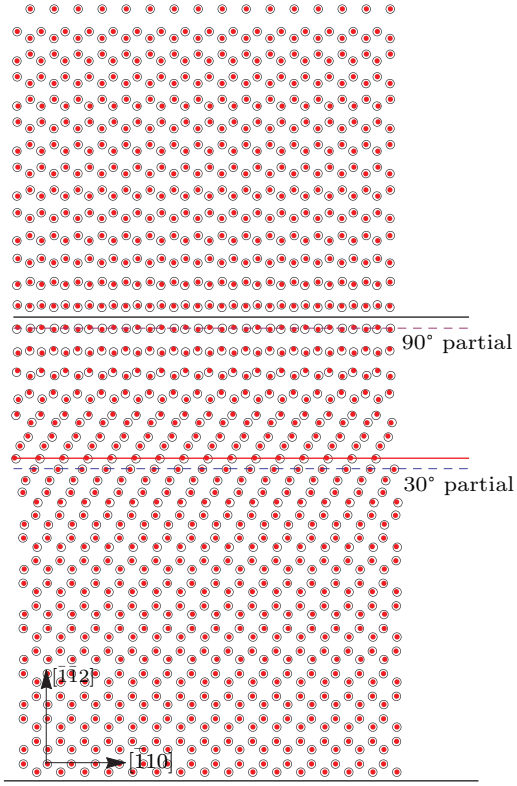


Fig. 16. The atom alignments on the *a*-plane and *b*-plane of the 60° dislocation given by the theory (big empty circles) and the first-principles calculation (small solid circles). There are 204 atoms in the super-cell used. The initial total energy is −725.666 eV and the final energy is −726.665 eV. The dotted and the solid lines are respectively used to label the partial dislocation centers obtained from the theory and the simulation. It seems that the core has a translation shift after relaxation.

In the first principle simulation, the supercell is constructed layer by layer. Firstly the nearest neighboring atom layer of the cut-plane, the *a*-layer (*a*-plane) and the *b*-layer (*b*-plane) are obtained from the slip field or displacement field. Because the atom aligned periodically along the dislocation line, we take a period as the width of the layers. The layer size in direction perpendicular to the dislocation line is taken to be $20b \approx 14a$, which is much larger that the core size ($\sim 5a$). The layer next to the *a*-layer (or *b*-layer) can be obtained similarly and the other layers can be added one by one continuously. The total layer number is 6 in our supercell. The supercell constructed is a prism that contains an isolated dislocation. Out of the prism, there is a 10 Å thick vacuum layer. In our calculations, a fixed out shell is chosen suitably to eliminate the surface effects, and the interior atoms are fully relaxed. The final simulation results are shown in Figs. 15–17. It can be seen that the theoretical predictions are considerably well confirmed by the first principle simulation except that the core of the 60° dislocation has a small shift after relaxation.

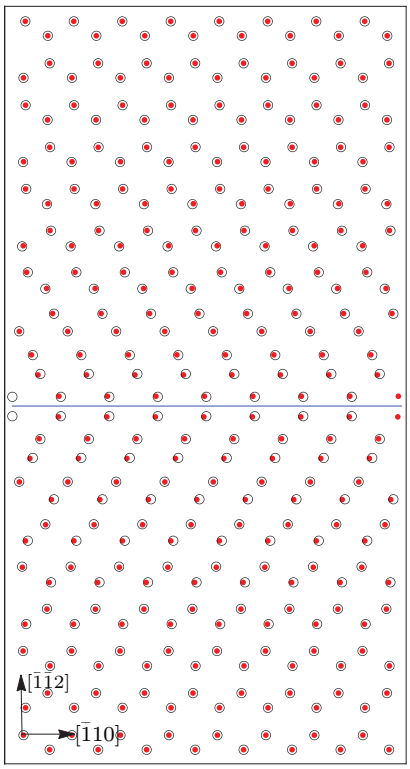


Fig. 17. The atom alignments on the *a*-plane and *b*-plane of the screw dislocation given by the theory (big empty circles) and the first-principles calculation (small solid circles). There are 108 atoms in the super-cell used. The initial total energy is −371.286 eV and the final energy is −371.479 eV. The energy drop is 0.193 eV in the relaxation process.

8. Conclusions

In summary, for temperature range $0 \leq T \leq 900$ K the core structure, the core energy and the Peierls stress are investigated for the 90° dislocation and 60° dislocations in Al using the fully discrete Peierls model. For the 90° dislocation, the core clearly dissociates into two partial dislocations with the separating distance $D \sim 12$ Å, which is larger than that ($3b$) obtained in Ref. [29]. The characteristic width of the partial dislocations is about 8 Å for the edge component. As for the screw component, there are two characteristic lengthes: one is about 6.5 Å, and the other is about 9.5 Å. The Peierls stress is very small $\sigma_p < 1$ kPa due to the large characteristic width and the small step length of the 90° dislocation. The 60° dislocation dissociates into the 30° and the 90° partial dislocations with the separating distance $D \sim 11$ Å, and the Peierls stress is about several MPa. Due to the asymmetric feature of the 60° dislocation, the core structure is more complex than that of the edge dislocation. The minimum characteristic length is about

5 Å and the maximum characteristic length is about 12 Å. The stress distribution is calculated by virtue of the superposition principle. The maximum stress on the misfit plane is as large as 0.1μ for all types of the dislocations. The core structures predicted theoretically at $T = 0$ K are confirmed by numerical simulation based on the electron density functional theory. The satisfactory agreement between the theoretical predictions and the first principle simulations indicates that the results presented are accurate and reliable. For both the 90° dislocation and 60° dislocations, no stability transformation in the core structure is observed in the temperature range $0 \leq T \leq 900$ K while there is stability transformation at $T \sim 700$ K for the screw dislocation.[36] The reason is unclear and needs to be explored further. From Table 1, one can see that the physics parameters in the energy functional change remarkably as temperature increases. However, because the changes of all parameters have the same tendency to become small and the equilibrium dislocation core mainly depends on the rescaled values of those parameters, the characteristic lengths of the dislocation cores given in Tables 2–5 change a little as temperature increases. Compared to the weak dependence of the core structure on temperature, the self energy E_{i} (interaction energy of the infinitesimal dislocations) and the misfit energy E_γ fall off significantly as temperature increases. As shown in Fig. 11, for all the three types of dislocations, the drops in self energy E_{i} and the misfit energy E_γ are approximately as large as one third when temperature increases from $T = 0$ K to $T = 900$ K. Therefore, as a sum of the self energy and the misfit energy, the dislocation energy at high temperature has an observable reduction compared with that at low temperature. In addition, it is notable that the Peierls stress of the 60° dislocation grows up from 1 MPa to 2 MPa as the temperature increases from 0 K to 900 K.

Acknowledgement

Project supported by the National Natural Science Foundation of China (Grant Nos. 11874093 and 11974062).

References

[1] Hirth J P and Lothe J 1982 *Theory of dislocations*, 2nd edn. (New York: Wiley)
[2] Cai W, Bulatov V V, Chang J, Li J and Yip S 2004 *Dislocations in Solids* vol. 12 pp. 1–80
[3] Billinge S J L and Levin I 2007 *Science* **316** 561
[4] Barnard J S, Sharp J, Tong J R and Midgley P A 2006 *Science* **313** 319
[5] Wang Z, Saito M, McKenna K P and Ikuhara Y 2014 *Nat. Commun.* **5** 3239
[6] Chen C, Wang Z, Kato T, Shibata N, Taniguchi T and Ikuhara Y 2015 *Nat. Commun.* **6** 6327
[7] Woodward C, Trinkle D R, Hector L G and Olmsted D L 2008 *Phys. Rev. Lett.* **100** 045507
[8] Fang Q F and Wang R 2000 *Phys. Rev. B* **62** 9317
[9] Szajewski B A, Hunter A, Luscher D J and Beyerlein I J 2017 *Modelling Simul. Mater. Sci. Eng.* **26** 015010
[10] Fu T, Peng X, Weng S, Zhao Y, Gao F, Deng L and Wang Z 2016 *Mater. Sci. Eng. A* **658** 1
[11] Fu T, Peng X, Wan C, Lin Z, Chen X, Hu N and Wang Z 2017 *Appl. Surf. Sci.* **392** 942
[12] Peierls R 1940 *Proc. Phys. Soc.* **52** 34
[13] Nabarro F 1947 *Proc. Phys. Soc.* **59** 256
[14] Christian J W and Vitek V 1970 *Rep. Prog. Phys.* **33** 307
[15] Wu X Z, Wang R, Wang S F and Wei Q Y 2010 *Appl. Surf. Sci.* **256** 6345
[16] Lejćcek L 1976 *Czech. J. Phys.* **26** 294
[17] Wang S F 2015 *Philos. Mag.* **95** 3768
[18] Lejćcek L and Kroupa F 1976 *Czech. J. Phys. B* **26** 528
[19] Ngan A H W 1997 *J. Mech. Phys. Solids* **45** 903
[20] Wang S and Hu X 2018 *J. Mech. Phys. Solids* **114** 75
[21] van der Merwe J H 1963 *J. Appl. Phys.* **34** 117
[22] Dundurs J 1968 *J. Appl. Phys.* **39** 4152
[23] Zhang S J and Wang S F 2020 *Chin. Phys. B* **29** 056102
[24] Joós B, Ren Q and Duesbery M S 1994 *Phys. Rev. B* **50** 5890
[25] Schoeck G 2005 *Mater. Sci. Eng. A* **400–401** 7
[26] Xiang Y, Wei H, Ming P and E W 2008 *Acta Mater.* **56** 1447
[27] Wang R, Wang S F and Wu X Z 2011 *Phys. Scr.* **83** 045604
[28] Wang R, Wang S F, Wu X Z and Wei Q Y 2010 *Phys. Scr.* **81** 065601
[29] Jiang Y Z, Wang R and Wang S F 2016 *Philos. Mag.* **96** 2829
[30] Bulatov V V and Kaxiras E 1997 *Phys. Rev. Lett.* **78** 4221
[31] Wang S F 2002 *Phys. Rev. B* **65** 094111
[32] Wang S F 2008 *J. Phys. A: Math. Theor.* **41** 015005
[33] Wang S F, Zhang S J, Bai J H and Yao Y 2015 *J. Appl. Phys.* **118** 244903
[34] Wang S F, Huang L L and Wang R 2016 *Acta Mater.* **109** 187
[35] Huang L L, Wang R and Wang S F 2018 *Philos. Mag.* **99** 347
[36] Xiang H, Wang R and Wang S F 2020 *J. Appl. Phys.* **127** 125106
[37] Wang Z, Saito M, McKenna K P and Ikuhara Y 2014 *Nat. Commun.* **5** 3239
[38] Shen C and Wang Y 2004 *Acta Mater.* **52** 683
[39] Parameswaran V R, Urabe N and Weertmant J 1972 *J. Appl. Phys.* **43** 2982
[40] Olmsted D L, HectorJr L G, Curtin W A and Clifton R J 2005 *Model. Simul. Mater. Sci. Eng.* **13** 371
[41] Srinivasan S G, Liao X Z, Baskes M I, McCabe R J, Zhao Y H and Zhu Y T 2005 *Phys. Rev. Lett.* **94** 125502
[42] Wang R, Wang S F and Wu X Z 2011 *Phys. Scr.* **83** 045604
[43] Mianroodi J, Hunter A, Beyerlein I and Svendsen B 2016 *J. Mech. Phys. Solids* **95** 719
[44] Lu G, Kioussis N, Bulatov V V and Kaxiras E 2001 *Mater. Sci. Eng. A* **309–310** 142
[45] Schoeck G 2003 *Mater. Sci. Eng. A* **356** 93
[46] Mryasov O, Gornostyrev Y and Freeman A 1998 *Phys. Rev. B* **58** 11927
[47] Schoeck G 2012 *Mater. Sci. Eng. A* **558** 162
[48] Zhou X W and Foster M E 2021 *Phys. Chem. Chem. Phys.* **23** 3290
[49] Wang S F 2009 *J. Phys. A: Math. Theor.* **42** 025208
[50] Xu S, Mianroodi J, Hunter A, Beyerlein I and Svendsen B 2019 *Philos. Mag.* **99** 1
[51] Kuksin A, Stegalov V and Yanilkin A 2008 *Dokl. Phys.* **53** 287
[52] Joós B and Duesbery M S 1997 *Phys. Rev. Lett.* **78** 266
[53] Wang S F, Li S R and Wang R 2011 *Eur. Phys. J. B* **83** 15
[54] Kosugi T and Kino T 1989 *J. Phys. Soc. Jpn.* **58** 4269
[55] Bulatov V V, Richmond O and Glazov M V 1999 *Acta Mater.* **47** 3507
[56] Hu X and Wang S F 2017 *Philos. Mag.* **98** 484
[57] Huang L L and Wang S F 2019 *J. Appl. Phys.* **125** 145702
[58] Kresse G and Hafner J 1993 *Phys. Rev. B* **48** 13115
[59] Kresse G and Furthmüller J 1996 *Comput. Mater. Sci.* **6** 15
[60] Kresse G and Furthmüller J 1996 *Phys. Rev. B* **54** 11169